J. Fluid Mech. (2018), *vol.* 837, R2, doi:10.1017/jfm.2017.895

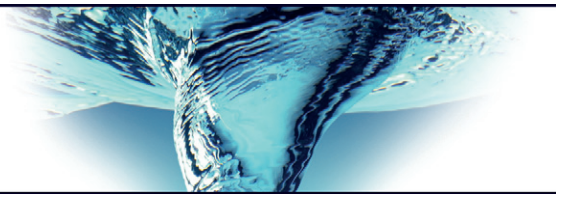

JFM RAPIDS
journals.cambridge.org/rapids

Lift on a steady 2-D symmetric airfoil in viscous uniform shear flow

Patrick R. Hammer[1],†, Miguel R. Visbal[2], Ahmed M. Naguib[1] and Manoochehr M. Koochesfahani[1]

[1]Department of Mechanical Engineering, Michigan State University, East Lansing, MI 48824, USA

[2]Aerospace Systems Directorate, Air Force Research Laboratory, Wright-Patterson Air Force Base, OH 45433, USA

(Received 23 October 2017; revised 6 December 2017; accepted 6 December 2017)

We present an investigation into the influence of upstream shear on the viscous flow around a steady two-dimensional (2-D) symmetric airfoil at zero angle of attack, and the corresponding loads. In this computational study, we consider the NACA 0012 airfoil at a chord Reynolds number 1.2×10^4 in an approach flow with uniform positive shear with non-dimensional shear rate varying in the range 0.0–1.0. Results show that the lift force is negative, in the opposite direction to the prediction from Tsien's inviscid theory for lift generation in the presence of positive shear. A hypothesis is presented to explain the observed sign of the lift force on the basis of the asymmetry in boundary layer development on the upper and lower surfaces of the airfoil, which creates an effective airfoil shape with negative camber. The resulting scaling of the viscous effect with shear rate and Reynolds number is provided. The location of the leading edge stagnation point moves increasingly farther back along the airfoil's upper surface with increased shear rate, a behaviour consistent with a negatively cambered airfoil. Furthermore, the symmetry in the location of the boundary layer separation point on the airfoil's upper and lower surfaces in uniform flow is broken under the imposed shear, and the wake vortical structures exhibit more asymmetry with increasing shear rate.

Key words: aerodynamics

1. Introduction

Current understanding of airfoil aerodynamics is based primarily on a uniform free-stream velocity approaching the airfoil. There are many situations, however, where significant disturbances are encountered during flight such that the condition of

† Email address for correspondence: hammerpa@egr.msu.edu

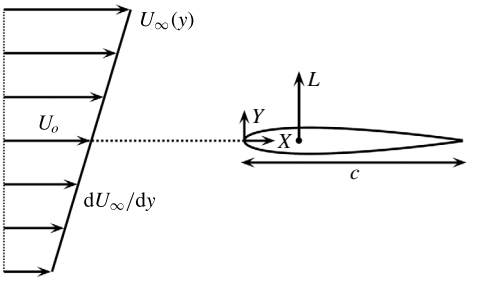

FIGURE 1. Schematic of flow geometry considered by Tsien (1943).

a uniform approach velocity is a very poor approximation. These situations include wings near the ground, wind shear, ambient wind conditions that are altered by large-scale disturbances (e.g. mountains), and aircraft operating in close proximity, among others. The work of Tsien (1943) was among the earliest to investigate the influence of non-uniform upstream conditions by considering a linear velocity profile (i.e. uniform shear) approaching a steady 2-D symmetric Joukowsky airfoil. The control parameter in this case is the non-dimensional shear rate, defined by Tsien as $K = (c/U_o)\,\mathrm{d}U_\infty/\mathrm{d}y$ (see figure 1 for a sketch of the flow geometry and description of the variables). Tsien's inviscid analysis showed that the effect of uniform shear is a shift in the zero-lift angle of attack (AoA). An essential conclusion was that a symmetric airfoil at zero AoA that is immersed in an approach flow with positive shear generates positive lift, i.e. the zero-lift AoA that would be normally zero in the case of uniform flow shifts to a negative AoA in the case of positive shear. Additionally, the magnitude of generated lift at zero AoA increases with shear rate. The work of Tsien was subsequently extended to more general velocity profiles in several studies, all of which are again limited to inviscid flows. Systematic studies of the influence of upstream shear on airfoil aerodynamics in real viscous flows are hard to find. One exception is the wind tunnel experiments of Payne & Nelson (1985) on a steady airfoil in uniform shear at chord Reynolds numbers on order of 10^5. It is difficult to conclusively determine the influence of shear on lift at zero AoA based on the reported data.

In view of the lack of knowledge described earlier, this work examines how the basic flow characteristics of steady airfoils, and the corresponding loads, are altered when the upstream approach flow is changed from the traditional uniform conditions to that of non-uniform flow. The particular focus of the current paper is to consider the viscous flow around a steady 2-D symmetric airfoil at zero AoA, and to assess Tsien's inviscid theory for lift generation in the presence of shear. We consider the NACA 0012 airfoil at a chord Reynolds number $Re_c = U_o c/\nu = 1.2 \times 10^4$ (where ν represents the kinematic viscosity), for which a great deal of experimental and computational data are available when the upstream flow is uniform. A computational approach is used here to obtain the loads on the airfoil over a range of non-dimensional shear rates K, along with details of the flow field around, and in the wake of the airfoil. In addition to comparing the lift force against the inviscid prediction, the data also allow us to quantify and report the various asymmetries in the flow that arise as a result of imposed shear (e.g. boundary layer separation location, wake structure, etc.), the type of information that is not available from inviscid theory.

2. Computational considerations

2.1. Governing equations and numerical method

The computations are performed using the full, compressible, unsteady, 2-D Navier–Stokes equations cast in strong conservative form after introducing a general time-dependent curvilinear coordinate transformation from physical to computational space (Vinokur 1974; Steger 1978; Tannehill, Anderson & Pletcher 1997). These equations are augmented using the perfect gas relationship, a constant Prandtl number, Sutherland's viscosity law and Stokes' hypothesis for the bulk viscosity coefficient.

All simulations are performed with the extensively validated high-order Navier–Stokes solver FDL3DI (Gaitonde & Visbal 1998; Visbal & Gaitonde 1999), the salient features of which are given briefly below. A finite-difference approach is employed to discretize the governing equations, and all spatial derivatives are obtained with high-order compact-differencing schemes (Lele 1992). A sixth-order scheme is used here at interior points, whereas at boundary points, higher-order one-sided formulae are invoked which retain the tridiagonal form of the scheme (Gaitonde & Visbal 1998; Visbal & Gaitonde 1999).

In order to eliminate spurious components, a high-order, low-pass spatial filter (Gaitonde & Visbal 1998; Visbal & Gaitonde 1999) is incorporated. This filtering approach is based on templates proposed in Alpert (1981) and Lele (1992), and with proper choice of coefficients provides up to tenth-order accuracy. Filter operators, along with representative filter transfer functions, can be found in Gaitonde & Visbal (1998) and Gaitonde & Visbal (1999). The filter is applied here to the conserved variables along each transformed coordinate direction using an interior eighth-order filter with filter coefficient $\alpha_f = 0.4$. At near-boundary points, the filtering strategies described in Gaitonde & Visbal (1999) and Visbal & Gaitonde (1999) are used. Finally, time marching is accomplished by incorporating an iterative, implicit approximately factored procedure (Beam & Warming 1978; Pulliam & Chaussee 1981; Visbal & Gaitonde 2002; Visbal, Morgan & Rizetta 2003).

The inviscid solution of the NACA 0012 airfoil in uniform shear is computed using an in-house panel code based on Katz & Plotkin (2001). Each panel has a vorticity distribution that varies linearly in strength along the panel. The only difference in this implementation of the panel method from Katz & Plotkin is that the traditional uniform free stream U_∞ is replaced by the imposed spatially varying free stream $U_\infty(y)$. The velocity from the approach flow at each panel depends only on the panel y-coordinate. The accuracy of the panel code is verified by comparing its prediction against the exact solution of Tsien (1943) for the Joukowsky airfoil in uniform shear.

2.2. Flow and computational parameters

The various computational parameters (grid resolution, time-step resolution, Mach number, etc.) given in this section are based on previous extensive convergence studies by Hammer (2016) for the case of uniform approach velocity and additional confirmation for the highest shear rate of $K = 1.0$ considered here. Details are not shown for brevity.

The geometry considered is a NACA 0012 airfoil with a rounded trailing edge ($r_{TE} = 2.2 \times 10^{-3}c$). An overset computational grid is used for this work (see figure 2). An O-grid (figure 2*a*) wraps around the airfoil with dimensions 655×165, leading edge spacing $\Delta\xi_{LE} = 5.0 \times 10^{-4}c$, trailing edge spacing $\Delta\xi_{TE} = 2.5 \times 10^{-4}c$, and initial normal spacing at the wall $\Delta\eta_{wall} = 5.0 \times 10^{-5}c$. A single Cartesian background grid

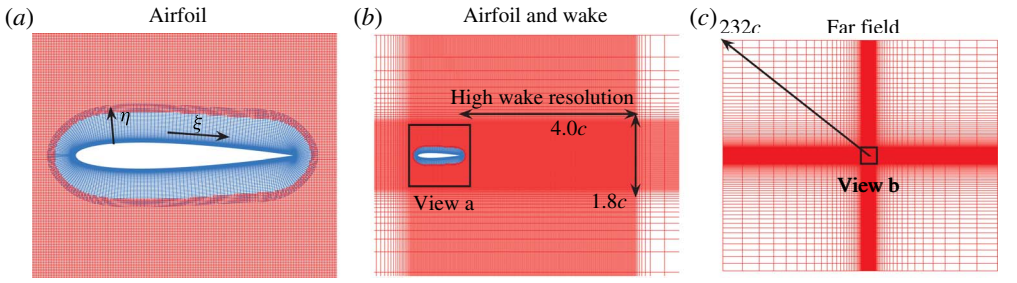

FIGURE 2. Schematic of computational domain, showing three fields of view. In views (*a*) and (*b*), grid points have been removed for clarity.

is used to maintain the shear profile while resolving the wake structure with high spatial resolution (figure 2*b*,*c*). Holes are cut in the background grid to blank out the region of the background grid coincident with the O-grid. The high-resolution wake region covers four chord lengths downstream of the trailing edge in the streamwise direction and 1.8 chord lengths in the transverse direction with a uniform spacing of $2.5 \times 10^{-3}c$. The Cartesian grid is then rapidly stretched to over 100 chords in each direction. This stretching along with the high-order filter helps eliminate spurious reflections off the boundary (Visbal & Gaitonde 1999). Grid communication and low-order interpolation is performed as a pre-processing step using Pegasus 5 (Suhs, Rogers & Dietz 2002), which is then extended to high order (Sherer & Scott 2005; Sherer & Visbal 2007).

The boundary conditions are prescribed as follows. A no-slip, adiabatic condition is applied to the surface in conjunction with a zero-normal pressure gradient at the wall. A prescribed streamwise velocity profile $U_\infty(y)$, uniform static pressure, and uniform total temperature are specified along the upstream far-field boundary. At the three additional far-field boundaries, a first-order accurate extrapolation condition is applied to the primitive variables, except for pressure, which is uniform. Spatial periodicity is enforced in the azimuthal direction of the O-mesh using a five-point overlap. The solution is initialized with the specified velocity profile, uniform static pressure, and uniform total temperature everywhere in the domain.

The inviscid theory by Tsien (1943) is based on a shear profile that extends to infinity, a boundary condition that is difficult to reproduce in the current computations since at high enough shear rates the velocities, and corresponding Mach numbers, become extremely large away from the airfoil (positive in the upper domain and negative in the lower). It is also incredibly challenging to create the equivalent boundary condition for experiments, especially the reverse flow profile below the airfoil. Therefore, our work utilizes a three-segment profile as the boundary condition, where the uniform shear zone (and its linear velocity profile) occurs over a finite region of thickness δ and the velocities outside this region are uniform. The details are shown schematically in figure 3. This composite profile is now characterized by the non-dimensional shear rate $K = (c/U_o)\,\mathrm{d}U_\infty/\mathrm{d}y$ introduced by Tsien (1943) and the new parameter δ/c. The results we discuss in this paper are for large enough δ/c such that the finite size of the shear zone does not influence the outcome.

The chord Reynolds number in this study is 1.2×10^4 based on the chord length c, and centreline velocity U_o. The non-dimensional shear rate K varies between 0.0 (uniform flow) and 1.0. Data are primarily presented here for the case of $\delta/c = 1.5$, determined to be large enough to make the results insensitive to increasing δ/c

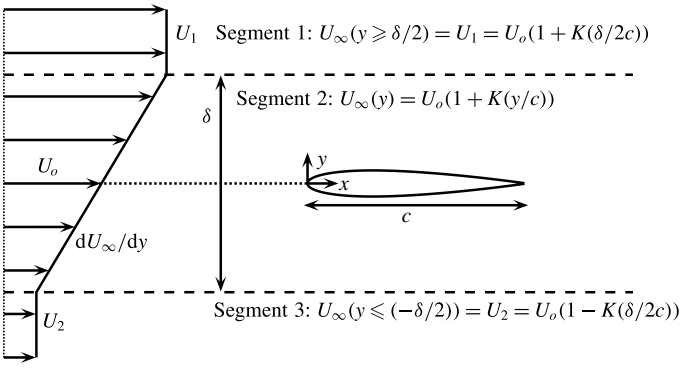

FIGURE 3. Schematic of three-segment linear velocity profile used for the upstream boundary condition in the current computations.

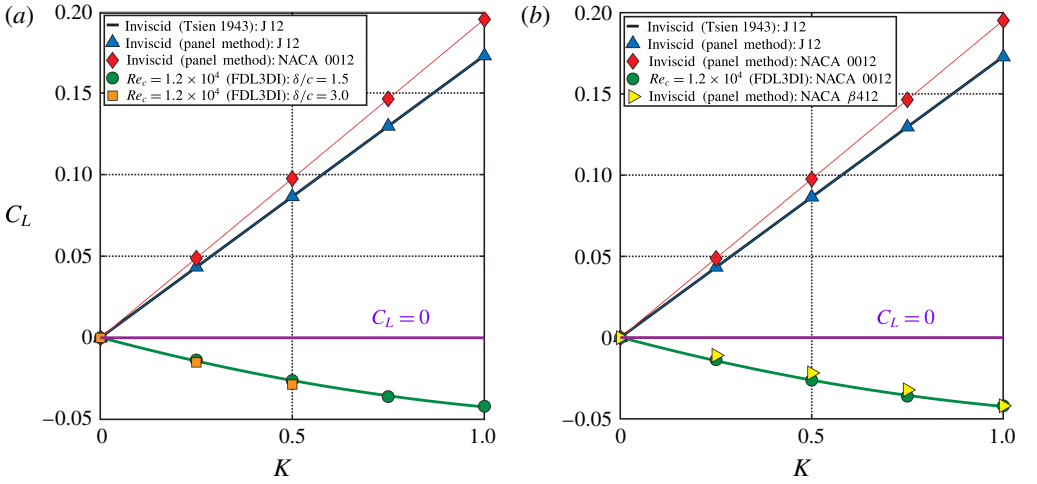

FIGURE 4. (*a*) Average lift coefficient C_L versus shear rate K for the NACA 0012 airfoil at $Re_c = 1.2 \times 10^4$ in comparison to the inviscid solution. The inviscid NACA 0012 and 12 %-thick Joukowsky airfoil (J 12) solutions are both included. (*b*) Comparison of the inviscid solution of the negatively cambered NACA β412 airfoil with the viscous solution of the NACA 0012 airfoil at $Re_c = 1.2 \times 10^4$. Maximum camber $\beta = 2\,\%$ at $K = 1.0$ and linear K scaling is used to obtain β for other K values.

(see figure 4*a*). Based on the previous work by Hammer (2016), a low reference Mach number M_o of 0.015 is selected to simulate the incompressible limit using the current compressible flow Navier–Stokes solver. The wake of the airfoil at the Reynolds number of this study is unstable and leads to a nearly periodic flow field and load. The solution is advanced in time with a non-dimensional time step ($\Delta\tau = \Delta t U_o/c$) of 5.0×10^{-5} with five subiterations per time step. Once the cycle-to-cycle variation in average lift and drag reaches less than 1 %, data are averaged over a single cycle using the period of lift fluctuation.

2.3. *Validation*

Validation of the current results is presented for the uniform flow case against existing data from experiments (Laitone 1997) and computations (Liu & Kawachi 1999; Young

Source	C_D
Current	0.0350
Laitone (1997): $C_D = 0.35Re_c^{-0.25}$	0.0334
Liu & Kawachi (1999)	0.0346
Young & Lai (2004)	0.0361

TABLE 1. Comparison of C_D for NACA 0012 at $Re_c = 1.2 \times 10^4$ and AoA $= 0°$ in uniform flow.

& Lai 2004). Comparison of the drag coefficient C_D shown in table 1 illustrates the very good agreement between the current results and published literature. The average lift is zero in all these studies and is not useful for validation purposes. In addition, the wake natural shedding frequency in the current computations is found to be within 2 % of the value from experiments by Koochesfahani (1989), and in exact agreement with the value from computations of Young & Lai (2004) at the same Re_c.

3. Results and discussion

3.1. *Average load on airfoil*

The average lift coefficient C_L at zero AoA versus shear rate K is shown in figure 4(*a*) for the viscous solution of the NACA 0012 airfoil at $Re_c = 1.2 \times 10^4$ in comparison to its inviscid solution using the panel method. The accuracy of the panel code is demonstrated to be excellent when tested against Tsien's exact solution for a 12 %-thick Joukowsky airfoil (J 12); see figure 4(*a*). Note that the inviscid C_L for the NACA 0012 airfoil increases linearly with K just as the 12 %-thick Joukowsky airfoil, but with a slope that is higher by 12.8 %, a consequence of the shape difference between these airfoils.

The most important result from figure 4(*a*) is that the behaviour of the viscous solution is fundamentally different from its inviscid counterpart. In the former, the sign of lift is negative (i.e. downward force), which is exactly the opposite of the inviscid prediction. Its magnitude, however, increases with shear rate K in a nearly linear fashion. We note in figure 4(*a*) that increasing the size of the shear zone by a factor of two to $\delta/c = 3.0$ has a minimal impact on the lift force, supporting the earlier assertion in § 2.2 that $\delta/c = 1.5$ is a sufficiently large value (highest values of K were not computed for $\delta/c = 3.0$ as it led to back flow in the approach stream on the low-speed side). The influence of upstream shear on the drag coefficient is found to be weak; results (not shown here) indicate that C_D decreases monotonically with increasing K, with C_D at $K = 1.0$, dropping by only 2 % compared to its value for uniform flow ($K = 0.0$).

Our hypothesis for generation of negative lift at zero AoA for a symmetric airfoil placed in a flow with positive shear is connected to the asymmetry of boundary layer development on the upper and lower surfaces of the airfoil. In positive shear, the upper boundary layer grows in a region with higher free-stream velocity compared to that on the lower surface, resulting in a thicker boundary layer on the lower surface than the upper surface. The resulting difference between the corresponding displacement thicknesses effectively creates an airfoil with negative camber (camber towards the low-speed side), leading to negative lift.

We now provide a first-order estimate of the resulting effect using laminar boundary layer relations for attached flow. The upper and lower surface boundary layer displacement thicknesses (δ_U^* and δ_L^*) at a given downstream location on the airfoil surface are given as $\delta_U^*/c \sim \sqrt{\nu/(cU_U)}$ and $\delta_L^*/c \sim \sqrt{\nu/(cU_L)}$, where U_U and U_L correspond to the characteristic free-stream velocities for boundary layer growth on the upper and lower surfaces, which can be written as $U_U \sim U_o(1 + Kt/2c)$ and $U_L \sim U_o(1 - Kt/2c)$, respectively, with t representing the airfoil thickness. The resulting 'effective' camber $y_c = (\delta_U^* - \delta_L^*)/2$ can be simplified for $K(t/2c) \ll 1$ to the following expression

$$\frac{y_c}{c} \sim -\frac{1}{\sqrt{Re_c}} K \left(\frac{t}{2c}\right). \tag{3.1}$$

Classical inviscid flow analysis of cambered Joukowsky airfoil (e.g. see chap. 4 of Currie 1993) connects the lift due to camber to the maximum camber of the mean camber line, which for small values of camber reduces to a linear relation between lift and maximum camber. Using this connection as a guide, we would estimate the *additional* lift caused by the effective camber described earlier to be negative and given as

$$C_L \sim -\frac{1}{\sqrt{Re_c}} K \left(\frac{t}{2c}\right). \tag{3.2}$$

We note that the effective camber, and therefore also the resulting lift magnitude, in this first-order model, is linear in both shear rate K and airfoil thickness ratio t/c and decreases as $1/\sqrt{Re_c}$.

In this description, the lift of a symmetric airfoil at zero AoA in viscous flow with positive shear will always be lower than its inviscid counterpart (i.e. Tsien's theory) by the expression given above. The results in figure 4(*a*) for $Re_c = 1.2 \times 10^4$ imply that the lift reduction due to negative camber at this Reynolds number is large enough to change the positive lift prediction of Tsien's theory to negative lift. To get a sense of the magnitude of negative camber that is required to reproduce the viscous flow results in figure 4(*a*), we obtain the inviscid solution (using the panel method) of shear flow at $K = 1.0$ past a 12 %-thick cambered NACA airfoil. We find, for example, that the negatively cambered NACA 2412 airfoil (2 % maximum camber located at $0.4c$) reproduces the C_L value of the viscous solution at $K = 1.0$. Extending the inviscid computation to lower values of K, after applying the linear K scaling to obtain the corresponding maximum camber β (its location fixed at $0.4c$) leading to the NACA β412 series of airfoils, reproduces the viscous solution of C_L versus K in figure 4(*a*) remarkably well; see figure 4(*b*). We should emphasize that the family of cambered airfoil shapes NACA β412 we have described above is not unique for reproducing the viscous solution. A similar outcome can be achieved by placing the maximum camber at other locations than $0.4c$ and adjusting the value of maximum negative camber accordingly.

The model developed here also allows us to give an estimate for how high the chord Reynolds number should be before the inviscid theory of Tsien (1943) becomes applicable. From inviscid calculations, we first determine the lowest value of negative effective camber that is required to yield C_L versus K results that reach 90 % of Tsien's theory. The outcome in comparison with the already-established value of negative camber at $Re_c = 1.2 \times 10^4$, in conjunction with the $1/\sqrt{Re_c}$ scaling of

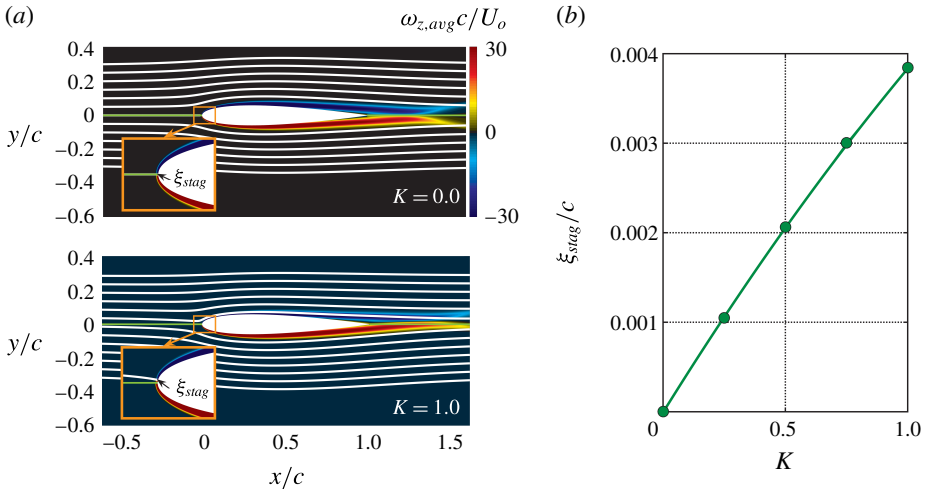

FIGURE 5. (*a*) Average streamlines and spanwise vorticity field ($\omega_{z,avg}c/U_o$) for uniform flow $K = 0.0$, shear flow $K = 1.0$ and front stagnation point location for each in a zoomed-up view of the leading edge. A green horizontal line at the centreline $y = 0$ originating at the airfoil leading edge is shown for reference. (*b*) The location of the front stagnation point, ξ_{stag}, for different shear rates.

effective camber, indicates that chord Reynolds number needs to be as high as $Re_c = 2 \times 10^6$ to get to 90 % of the inviscid prediction. It is important to recognize that the model given above and its prediction are constrained by its assumptions of thin laminar boundary layers and attached flow, which cease to be uniformly valid over the curved surfaces of the airfoil as the Reynolds number varies.

3.2. *Flow-field characteristics*

We now present some of the asymmetries that develop in the flow field due to the imposed shear. The time-averaged spanwise vorticity field, $\omega_{z,avg}c/U_o$, and accompanying streamline pattern are shown in figure 5(*a*) for uniform flow ($K = 0.0$) and the highest shear rate case ($K = 1.0$) studied here. For the symmetric airfoil in uniform flow, the stagnation streamline is aligned with the centreline ($y = 0$) and the front stagnation point is located at the leading edge, as expected. However, for the same symmetric airfoil placed in positive shear the stagnation streamline approaches the airfoil from above the centreline and the front stagnation point moves above the leading edge. The location of the stagnation point moves increasingly farther back along the upper surface with increased shear rate; see figure 5(*b*). The observed behaviour of the leading edge stagnation point is consistent with what is expected from an airfoil which, while geometrically symmetric, behaves effectively as a negatively cambered airfoil. As discussed in § 3.1, the magnitude of the effective (negative) camber increases with shear rate K, a consequence of which is the movement of the front stagnation point along the upper surface displayed in figure 5(*b*).

Another asymmetry that develops due to imposed shear is the location of boundary layer separation on the upper and lower surfaces, as illustrated in figure 6. For uniform

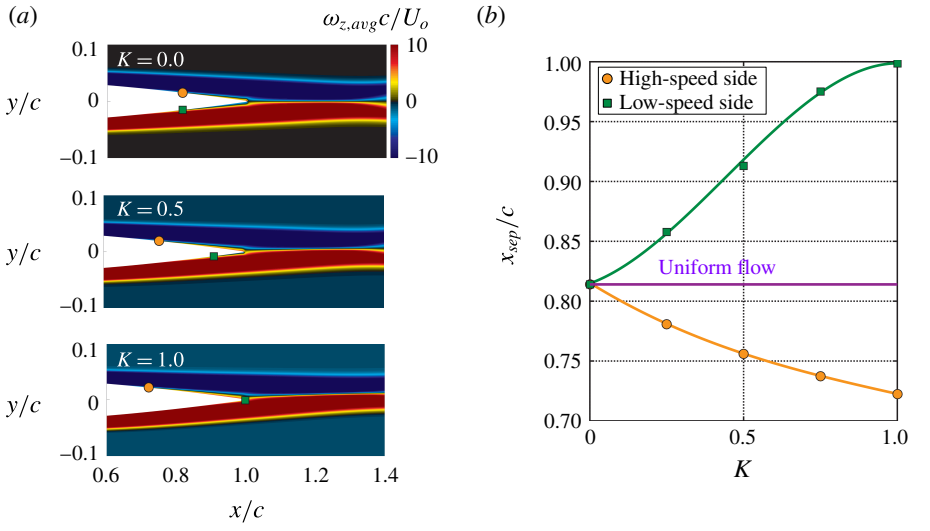

FIGURE 6. (*a*) Boundary layer separation points marked on the average spanwise vorticity field for different shear rates. (*b*) Average separation point location x_{sep} versus K. Solid lines represent curve fits to data.

flow ($K = 0.0$) past the NACA 0012 airfoil at $Re_c = 1.2 \times 10^4$, the boundary layers on the upper and lower surfaces remain attached until separation occurs symmetrically at $x_{sep}/c = 0.815$. The separation point is defined here as the location where the average surface shear stress reaches zero. When the approach flow has positive shear, the boundary layers develop asymmetrically on the upper and lower surfaces. Results show that as the shear rate K increases, the separation point on the upper surface (high-speed side) moves upstream. Conversely, the separation point on the lower surface (low-speed side) moves downstream, and at $K = 1.0$ reaches the trailing edge.

Finally, we present the changes that occur in the airfoil wake structure upon imposed shear; see figure 7. For uniform flow past the airfoil, the wake instability leads to the well-known formation of the Kármán vortex street (see top image of figure 7*a*). The natural shedding Strouhal number for uniform flow at the Reynolds number of this study is found to be $St_n \approx 2.7$, where $St_n = f_n c/U_o$ with f_n being the shedding frequency of the wake, which we obtain from the time history of the periodic lift fluctuation. The influence of upstream shear on the wake structure is captured in the instantaneous maps of the vorticity field, $\omega_z c/U_o$, in figure 7(*a*) for different shear rates K. For reference, the approach shear flow has a uniform negative vorticity given by $-K$. We note from figure 7(*a*) that as the shear rate increases, the vortical structures in the wake exhibit more asymmetry, with the negative vorticity getting stronger and positive vorticity getting weaker. Data for $K = 1.0$ indicate that at $x/c = 4$ (i.e. three chord lengths downstream of the airfoil trailing edge), the magnitudes of peak negative and positive vorticity have increased by 17 % and decreased by 54 %, respectively, compared to their magnitudes in uniform flow. Interestingly, however, the natural shedding Strouhal number depicted in figure 7(*b*) changes very little, only about 5 % increase, in going from $K = 0.0$ (uniform flow) to the highest shear rate $K = 1.0$.

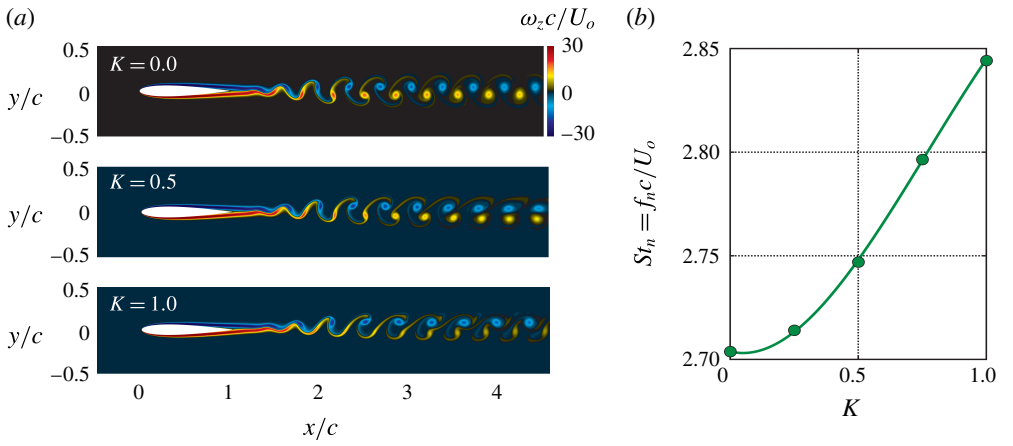

FIGURE 7. Influence of upstream shear on (*a*) the instantaneous spanwise vorticity field ($\omega_z c/U_o$) and (*b*) the natural shedding Strouhal number St_n. Solid line represents a curve fit to data.

4. Conclusions

The study presented here is our starting point in filling the knowledge gap in the influence of non-uniform approach flow on basic flow characteristics of airfoils, and the corresponding loads, which have been predominantly studied in the past by inviscid analysis. Current results at a chord Reynolds number of 1.2×10^4 have revealed several interesting flow-field asymmetries that develop as a result of imposed shear; information that is not available from inviscid theory. A discovery has been the negative sign of lift force on a symmetric airfoil at zero angle of attack when it is placed in an approach flow with positive shear; an effect that is the opposite of that expected from Tsien's inviscid theory. Our explanation for the underlying flow physics responsible for this effect argues for an airfoil that, while geometrically symmetric, effectively behaves as an airfoil with negative camber, which is caused by the asymmetric viscous boundary layer development on the airfoil upper and lower surfaces. We should mention that a comprehensive experimental study to complement the current computations is nearly complete, and recently reported preliminary results by Olson, Naguib & Koochesfahani (2016) corroborate the negative sign of the lift force reported here.

The simple model developed here to explain the negative camber effect provides information on its scaling with Reynolds number. According to the model, the chord Reynolds number needs to be as high as $Re_c = 2 \times 10^6$ in order to get to 90 % of inviscid prediction. This first-order model and its prediction are, however, constrained by its assumptions of thin laminar boundary layers and attached flow over the curved surfaces of the airfoil, which are not uniformly valid with variations in Reynolds number. A computational study is currently in progress to extend the current work to higher Reynolds numbers and determine the approach to the inviscid solution.

Acknowledgements

The authors would like to particularly thank S. Sherer, D. Garmann and C. Barnes of AFRL for their abundant assistance with FDL3DI and accompanying software

usage. The authors would also like to thank D. Olson for thoughtful discussions and technical assistance. This work was supported by AFOSR grant no. FA9550-15-1-0224. Partial support was provided by Michigan State University through the computational resources of the Institute for Cyber-Enabled Research.

References

ALPERT, P. 1981 Implicit filtering in conjunction with explicit filtering. *J. Comput. Phys.* **44**, 212–219.

BEAM, R. & WARMING, R. 1978 An implicit factored scheme for the compressible Navier–Stokes equations. *AIAA J.* **16** (4), 393–402.

CURRIE, I. G. 1993 *Fundamental Mechanics of Fluids*. CRC Press, Taylor & Francis Group.

GAITONDE, D. V. & VISBAL, M. R. 1998 High-order schemes for Navier–Stokes equations: algorithm and implementation into FDL3DI. *Tech. Rep.* Air Force Research Laboratory.

GAITONDE, D. V. & VISBAL, M. R. 1999 Further development of a Navier–Stokes solution procedure based on higher-order formulas. *AIAA Paper* 99-16436.

HAMMER, P. R. 2016 Computational study on the effect of Reynolds number and motion trajectory asymmetry on the aerodynamics of a pitching airfoil at low Reynolds number. PhD thesis, Michigan State University.

KATZ, J. & PLOTKIN, A. 2001 *Low-Speed Aerodynamics*, 2nd edn. Cambridge University Press.

KOOCHESFAHANI, M. M. 1989 Vortical patterns in the wake of an oscillating airfoil. *AIAA J.* **27** (9), 1200–1205.

LAITONE, E. 1997 Wind tunnel tests of wings at Reynolds numbers below 70 000. *Exp. Fluids* **23**, 405–409.

LELE, S. 1992 Compact finite difference scheme with spectral-like resolution. *J. Comput. Phys.* **103**, 16–42.

LIU, H. & KAWACHI, K. 1999 A numerical study of undulatory swimming. *J. Comput. Phys.* **155**, 223–247.

OLSON, D. A., NAGUIB, A. M. & KOOCHESFAHANI, M. M. 2016 Experiments on a steady low Reynolds number airfoil in a shear flow. *Bull. Am. Phys. Soc.* **61**, 174.

PAYNE, F. & NELSON, R. 1985 Aerodynamic characteristics of an airfoil in a nonuniform wind profile. *J. Aircraft* **22** (1), 5–10.

PULLIAM, T. & CHAUSSEE, D. 1981 A diagonal form of an implicit approximate-factorizarion algorithm. *J. Comput. Phys.* **39**, 347–363.

SHERER, S. & SCOTT, J. 2005 High-order compact finite difference methods on overset grids. *J. Comput. Phys.* **210**, 459–496.

SHERER, S. & VISBAL, M. 2007 Multi-resolution implicit large eddy simulations using a high-order overset grid approach. *Intl J. Numer. Meth. Engng* **55**, 455–482.

STEGER, J. 1978 Implicit finite-difference simulation of flow about arbitrary two-dimensional geometries. *AIAA J.* **16** (7), 679–686.

SUHS, N., ROGERS, S. & DIETZ, W. 2002 Pegasus 5: an automated pre-processor for overset-grid CFD. *AIAA Paper* 2002-3186.

TANNEHILL, J., ANDERSON, A. & PLETCHER, R. 1997 *Computational Fluid Mechanics and Heat Transfer*. Taylor & Francis.

TSIEN, H.-S. 1943 Symmetrical Joukowsky airfoils in shear flow. *Q. Appl. Maths* **1** (2), 130–148.

VINOKUR, M. 1974 Conservation equations of gas dynamics in curvilinear coordinate system. *J. Comput. Phys.* **14**, 105–125.

VISBAL, M., MORGAN, P. & RIZETTA, D. 2003 An implicit LES approach based on high-order compact differencing and filtering schemes (invited). *AIAA Paper* 2003-4098.

VISBAL, M. R. & GAITONDE, D. V. 1999 High-order-accurate methods of complex unsteady subsonic flows. *AIAA J.* **37** (10), 1231–1239.

VISBAL, M. R. & GAITONDE, D. V. 2002 On the use of higher-order finite-difference schemes on curvilinear and deforming meshes. *J. Comput. Phys.* **181**, 155–185.

YOUNG, J. & LAI, J. 2004 Oscillation frequency and amplitude effects on the wake of a plunging airfoil. *AIAA J.* **42** (10), 2042–2052.